

1 Organic matters, but inorganic matters too: column examination
2 of elevated mercury sorption on low organic matter aquifer
3 material using concentrations and stable isotope ratios.

4 David S. McLagan^{1,2,3,*}, Carina Esser^{1,*}, Lorenz Schwab^{4,5}, Jan G. Wiederhold⁴, Jan-
5 Helge Richard⁶, Harald Biester¹.

6 1 - Institute of Geoecology, Technische Universität Braunschweig, Braunschweig, 38106, Germany.

7 2 - Department of Geological Sciences and Geological Engineering, Queen's University, Kingston, ON, K7L3N6, Canada.

8 3 - School of Environmental Studies, Queen's University, Kingston, ON, K7L3J6, Canada.

9 4 - Department for Environmental Geosciences, Centre for Microbiology and Environmental Systems Science, University
10 of Vienna, Vienna, 1090, Austria.

11 5 - Environmental Engineering Institute IIE-ENAC, Soil Biogeochemistry Laboratory, Ecole Polytechnique Fédérale de
12 Lausanne (EPFL), Sion, Switzerland.

13 6 - Institute for Hygiene and Environment Hamburg, 20539 Hamburg, Germany

14 * - These authors contributed equally to the manuscript.

15

16 Abstract

17 Sorption of mercury (Hg) in soils is suggested to be predominantly associated with organic matter
18 (OM). However, there is a growing collection of research that suggests clay minerals and Fe/Mn-
19 oxides are also important solid-phases for the sorption of soluble Hg in soil-groundwater systems.
20 We use a series of (60 mL syringe based) column experiments to examine sorption and subsequent
21 desorption of HgCl₂ solutions (Experiment 1 [EXP1]: 46.1 ± 1.1 mg L⁻¹; and Experiment 2 [EXP2]: 144
22 ± 6 mg L⁻¹) in low OM (0.16 ± 0.02 %) solid-phase aquifer materials. Analyses of total Hg
23 concentrations, Hg speciation (i.e., pyrolytic thermal desorption (PTD)), and Hg stable isotopes are
24 performed on both solid- and liquid-phase samples across sorption and desorption phases.

25 Sorption breakthrough curve best fitted a Freundlich model. Despite the very low OM content, the
26 Hg equilibrium sorptive capacity in these columns is very high: 1510 ± 100 and 2320 ± 60 mg kg⁻¹ for
27 the EXP1 and EXP2, respectively, and is similar to those determined for high OM soils. Data from the
28 experiments on mass dependent fractionation of Hg stable isotope fractionation data (described by
29 δ²⁰²Hg) support preferential sorption of lighter isotopes to the solid-phase materials with results
30 indicating isotopically heavier liquid-phase and isotopically lighter solid-phase. Desorption fits
31 exponential decay models and 46 ± 6% and 58 ± 10% of the sorbed Hg is removed from the solid-
32 phase materials at the termination of desorption in EXP1 and EXP2, respectively. The divergence of
33 δ²⁰²Hg values between liquid- and solid-phase also continues into desorption. This desorption
34 profile is linked to the initial release of easily exchangeable Hg(II) species physically sorbed to
35 Fe/Mn-oxides and clay mineral surfaces (liquid-phase enriched in heavy isotopes) and then slower
36 release of Hg(II) species that have undergone secondary reaction to more stable/less soluble Hg(II)
37 species and/or diffusion/transport into the mineral matrices (processing favouring lighter isotopes;
38 solid-phase enriched in lighter isotopes). The secondary production of Hg(0) within the columns is
39 confirmed by PTD analyses that indicate distinct Hg(0) release peaks in solid-phase samples at <175
40 °C, which again agree with field observations. Retardation (R_D) and distribution (K_D) coefficients are
41 77.9 ± 5.5 and 26.1 ± 3.0 mL g⁻¹ in EXP1, respectively, and 38.4 ± 2.7 and 12.4 ± 0.6 mL g⁻¹ in EXP2,
42 respectively. These values are similar to values derived from column experiments on high OM soil
43 and provide the basis for future Hg fate and transport modelling in soil-groundwater systems.

44 **Keywords:** Mercury stable isotopes, column experiments, sorption/desorption, groundwater,
45 polluted sites, distribution coefficient.

46 1 Introduction

47 Mercury (Hg), a transition metal of group 12 and period 6 of the periodic table, has a unique
48 electrochemical structure. The pair of electrons in the outermost (6s) shell have a relativistically
49 contracted radius, which greatly reduces the element's ability to form metal-metal bonds (Norrby,
50 1991). Hence, Hg is the only liquid-phase metal at standard temperature and pressure. Even with
51 this radial contraction, Hg is an atomically large element, and species in its divalent oxidation state
52 qualify as "soft-acids", which under hard and soft Lewis acid and base theory results in Hg having
53 greater affinity for "soft-bases" (Ho, 1975). One particularly pertinent "soft-base" for Hg is sulphur.
54 Cinnabar (α-HgS) and meta-cinnabar (β-HgS) are the dominant forms of Hg in the lithosphere
55 (Gettens et al., 1972; Clarkson, 1997), but are relatively stable ores that have very low solubility,
56 and bioavailability (Llanos et al., 2011; Lu et al., 2011). Mining of these cinnabar ores for industrial
57 use of Hg has heavily perturbed the natural biogeochemical cycle of Hg. Other primary sources of
58 Hg emissions/releases to the environment include geogenic (natural), fossil-fuel combustion,

59 industrial and medical uses of Hg, and legacy emissions from Hg polluted sites (Pirrone et al., 2010;
60 Kocman et al., 2013; Streets et al., 2019).

61 While redox conditions and organic matter (OM) availability and composition are key determinants
62 in the mobility of Hg in aquatic/saturated subsurface environments, pH (Andersson, 1979; Gu et al.,
63 2011; Manceau and Nagy, 2019), chloride concentration (Cl^- ; Schuster, 1991), and speciation of Hg
64 inputs (particularly for polluted systems; McLagan et al., 2022) also play important roles. Solubilities
65 of Hg species vary widely from practically insoluble cinnabar species ($\approx 2 \cdot 10^{-24} \text{ g L}^{-1}$) to low solubility
66 elemental Hg ($\text{Hg}(0)$: $\approx 5 \cdot 10^{-5} \text{ g L}^{-1}$) to highly soluble Hg(II)-chloride (HgCl_2) (66 g L^{-1}) (Sanemasa,
67 1975; Schroeder and Munthe, 1998; Skyllberg et al., 2012). In systems that are OM limited, clay
68 minerals and oxides, hydroxides, and oxyhydroxides of Fe, Mn and Al become increasingly important
69 sorbents for Hg species (Lockwood and Chen, 1973; Schuster 1991; Kim et al., 2004). Additionally,
70 there is a strong tendency of Hg(II) to complex with hydroxides and halides under oxic conditions
71 (Schuster, 1991, Ullrich et al., 2001). Uptake of Hg to inorganic sorbents has been reported to occur
72 via rapid initial surface sorption followed by slower phase of Hg undergoing secondary
73 transformation to more stable/less soluble species or diffusing into the mineral matrices (Avotins,
74 1975; Miretzky et al., 2005; McLagan et al., 2022).

75 More recently, laboratory and field studies have expanded biogeochemical assays of Hg in
76 subsurface environments using stable isotopes (Jiskra et al., 2012; Zheng et al., 2018; McLagan et
77 al., 2022). Hg is an isotopic system that has seven stable isotopes and to which environmental
78 processes can impart mass-dependent (MDF) as well as both odd and even mass-independent (MIF)
79 fractionation (Bergquist and Blum, 2007; 2009; Wiederhold, 2015). In particular, this capacity for Hg
80 stable isotope analyses to elicit valuable information on tracing/identifying specific environmental
81 processes make them a vital tool in the examination of Hg biogeochemical cycling (Bergquist and
82 Blum, 2007; 2009; Wiederhold, 2015).

83 Traditionally, column and batch experiments have been utilised to assess the sorption (including
84 sorption or distribution coefficient: K_D and the related retardation coefficient: R_D) and mobility of
85 contaminants for solid-phase soil and aquifer materials. Both methods have strengths and
86 weaknesses. Batch experiments represent the simplest means to test analyte sorption, but these
87 experiments are static, and equilibrium oriented; questions about the applicability of the results to
88 natural systems with flowing water and potentially changing levels of saturation logically persist
89 (Schlüter et al., 1995 Schlüter, 1997; Van Glubt et al., 2022). Flow-through columns provide a much
90 more dynamic and manipulatable experimental environment that is also not exclusively limited to
91 equilibrium-based sorption simulations. Nonetheless, they are more laborious, difficult to replicate
92 from column to column, column boundaries (walls) can present preferential flow problems, and
93 despite the ability to manipulate the physicochemical properties of the columns this inevitably
94 underrepresents the inherent variability of actual soil/aquifer conditions (Sentenac et al., 2001;
95 USEPA, 2004). Soil contaminant transport modelling is a rapidly developing field of research and
96 provides an alternative/complementary method to these traditional experimental methods. While
97 Hg soil transport modelling is also advancing, progress is somewhat limited by the lack of
98 measurement data particularly relating to K_D values, Hg speciation and methods of assessing specific
99 processes for different soil/solid-phase materials (Leterme et al., 2014; Richard et al., 2016a).

100 Thus, it is important from both experimental and modelling standpoints that we determine effective
101 means of deriving information on sorption/mobility of Hg in soils. Lacking the capacity to measure
102 aquifer systems *in-situ*, we deem column experiments using solid-phase materials sourced from

103 sites of interest as the best available method to do so. Within this study, we aim to determine the
 104 sorptive (and desorptive) capacity of low OM aquifer materials for Hg(II) using column experiments
 105 and total Hg (THg) concentration, speciation, and stable isotope analyses of both solid and liquid-
 106 phase materials. These experiments will be the first conducted on such low OM soil/aquifer material
 107 and provide critical data into Hg transport and sorption within low OM soil and aquifer systems to
 108 improve our geochemical understanding of subsurface Hg behaviour and for soil chemistry and
 109 transport modelling. In addition, these column experiments on uncontaminated aquifer material
 110 sourced from an area adjacent to a former industrial site at which HgCl₂ was applied as wood
 111 preservative will simulate the contamination process. Data will aid our interpretation of the Hg
 112 biogeochemistry in coupled soil-groundwater systems, as well as future Hg groundwater transport
 113 modelling, and potentially provide guidance on contaminated site remediation.

114 2 Methods

115 2.1 Materials and experimental setup

116 The solid-phase material used in these experiments is highly permeable sand-gravel sediments
 117 sourced from the saturated zone of an unconsolidated aquifer (approximate depth: 10 m) extracted
 118 by a soil drill core in 2019. This site was impacted by losses of approximately 10-20 tonnes of Hg in
 119 the form of high concentration HgCl₂ solution ($\approx 0.66\%$ HgCl₂) that was applied to timber as a
 120 preservative (Schöndorf et al., 1999; Bollen et al., 2008; McLagan et al., 2022). The solid-phase
 121 materials were extracted from outside of the plume of contaminated groundwater (Site B in
 122 McLagan et al., 2022); and hence, the starting THg concentration within was very low (Table 1). The
 123 geology and structure of the soil/aquifer profile has been described in detail in previous works
 124 (Schöndorf et al., 1999; Bollen et al., 2008; McLagan et al., 2022). The material was stored in a dark
 125 and cool place before drying at 30 °C for 48 hours. It was then sieved to a size of <2 mm using a
 126 mesh soil sieve, which resulted in a distribution of $74.1 \pm 4.6\%$ coarse load (>2 mm; not used) and
 127 $25.8 \pm 4.6\%$ fine load (<2 mm). A subsequent particle size analysis of the fine load was carried out
 128 using sieving and sedimentation method (DIN ISO 11277, 2002), and results (see Table 1) categorise
 129 the solid-phase aquifer materials as a sandy-loam on the soil texture triangle. A summary of the
 130 properties of the investigated material is shown in Table 1.

131 *Table 1: Properties of the solid-phase aquifer material used.*

Parameter	Fe (g kg ⁻¹)	Mn (mg kg ⁻¹)	Hg (μ g kg ⁻¹)	TC (%)	TOC (%)	TIC (%)	Clay (%)	Silt (%)	Sand (%)
Value	19.2 \pm 1.5	690 \pm 160	20.4 \pm 1.0	0.50 \pm 0.03	0.16 \pm 0.02	0.34 \pm 0.03	13.5	23.2	63.3
Samples (n)	16	16	6	3	3	3	1	1	1

132

133 A set of preliminary experiments prior to experiment 1 (EXP1) and experiment 2 (EXP2) were run to
 134 optimise packing methods, flow rates, stock solution concentration, and time the experiments
 135 would take, and these are detailed in Section S1. Based on these preliminary data the experimental
 136 setup was based on a modified version of DIN method 19528-01 (DIN 2009). 8 x 60 mL disposable
 137 polypropylene syringes (height: 15.49 cm; inner diameter: 2.97 cm) were used as columns in each
 138 experiment (Figure 1). The insides of the columns were roughened with sandpaper (and thoroughly
 139 cleaned with surfactant and rinsed with deionised water to remove any debris) in order to minimise
 140 preferential flow along the walls of the column. Each column was then filled with a layer of quartz
 141 wool and a layer of quartz beads whose combined volume reached the 10 ml mark on the syringe.

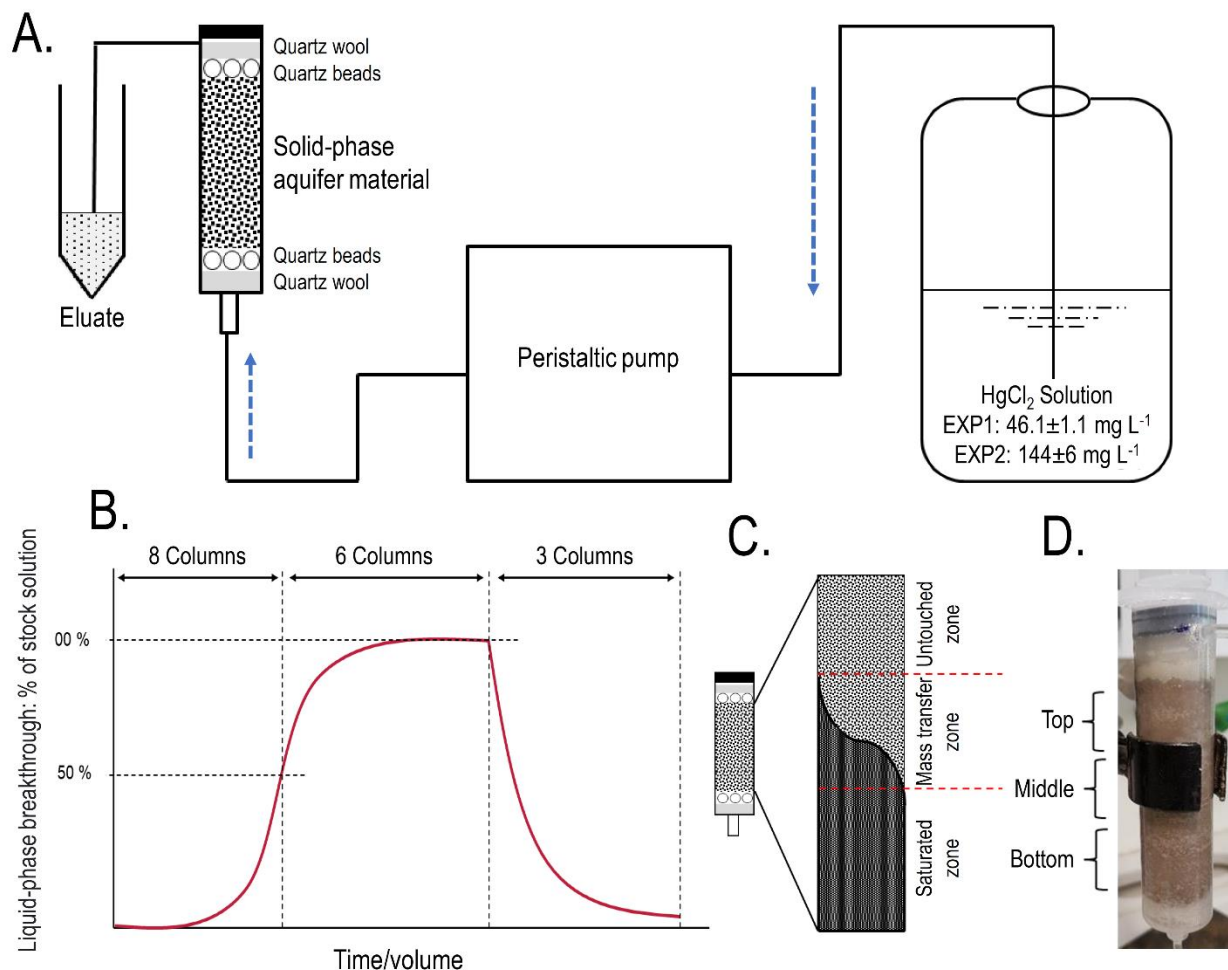
142 The sieved and dried material was then transferred by ≈ 14 g aliquots into the syringes (preliminary
143 testing revealed dry packing achieved optimal column density and was best at preventing
144 separation). Each aliquot was compacted to the desired volume and the surface of each aliquot was
145 broken up before the addition of the subsequent aliquot to prevent layering between each addition.
146 The mean mass and bulk density (ρ_b) of the solid-phase aquifer materials added to the columns was
147 70.09 ± 0.04 g and 1.42 ± 0.01 g cm⁻³, respectively, in EXP1, and 70.05 ± 0.03 g and 1.43 ± 0.01 g cm⁻³,
148 respectively, in EXP2. This resulted in the height of the solid-phase materials within the column
149 being ≈ 11 cm. Additional layers of quartz beads then quartz wool (syringe volume again ≈ 10 mL)
150 were added on top of the solid-phase materials to reduce column separation and particle transport.
151 Individual columns are named C1.1 to C1.8 for EXP1 and column C2.1 to C2.8 in EXP2. According to
152 Lewis and Sjöström (2010), the average bulk densities range from 1.2 – 2.0 g cm³ for sands and 1.6
153 – 2.0 g cm³ for gravel. Thus, we deem the achieved bulk density of the columns to be appropriate
154 for these materials, particularly as densities of the removed coarse materials are higher (solid
155 densities are estimated at 2.65 g cm³; Lewis and Sjöström (2010)).

156 All column experiments were conducted under saturated conditions. Figure 1A shows the
157 configuration of the setup with the peristaltic pump upstream of the columns and flow through the
158 columns was bottom to top to minimise entrapment of air and preferential flow paths. The stock
159 solution, peristaltic pump, columns, and eluate sampling points were connected with 3.125 mm
160 (inner-diameter) polypropylene tubing (length: 105 ± 10 cm; $n = 16$). To simulate the aquifer (flow
161 velocity of $\approx 3 - 10$ m day; Schöndorf et al., 1999; Bollen et al., 2008) and prevent separation of the
162 solid-phase materials within the column, the lowest possible volume flow of 0.62 ± 0.02 ml min⁻¹ (n
163 = 16) was set across all columns (flow velocities measured before and after experiments; Section
164 S2). The stock solution was made using mixing HgCl₂ salt with tap water and stored in a 20 L
165 polyethylene container. Tap water was selected due to its inherent concentration of ions, low
166 potential for biological activity, and ease-of-use (challenges in extraction, storage, and transport of
167 large groundwater volumes from study site ≈ 600 km away). Critically, the tap water and eluate DOC
168 concentrations ($2.3 - 3.3$ mg L⁻¹) were of a similar range (even slightly less) than the values measured
169 by Richard et al (2016a) at the site these solid-phase materials were removed ($3.8 - 6.3$ mg L⁻¹). This
170 should eliminate the possibility that tap water would introduce a significant amount of artificial
171 sorption sites associated with DOC being added to the system.

172 Stock solutions were 46.1 ± 0.1 mg L⁻¹ in EXP1 ($n = 6$) and 144 ± 6 mg L⁻¹ in EXP2 ($n = 12$) and were
173 selected for (i) experimental constraints/time considerations (see Figure S1.6) and (ii) these values
174 remain between HgCl₂ concentration applied during industrial activities (6600 mg L⁻¹; spillages of
175 this solution to the top of the soil profile) and recently measured groundwater concentrations up to
176 164 ± 75.4 μ g L⁻¹ observed 55 years after cessation of the industrial activities at the site (McLagan
177 et al., 2022). The physicochemical properties of both the stock solutions and eluate were monitored
178 across the experiments and data are listed in Section S2. Desorption was performed by replacing
179 the stock solution with tap water flowing at the same velocity. In total (sorption, equilibrium, and
180 desorption), EXP1 and EXP2 ran continuously for 14 days, 3 hours, and 9 minutes, and 10 days, 13
181 hours and 4 minutes, respectively.

182 Columns were pre-conditioned with tap water for 1 week at the experimental flow velocity to allow
183 equilibration between the solid-phase materials and the dissolved substances in the tap water, the
184 major component of the stock solution used within the experiment. After 24 hours of pre-
185 conditioning, NaCl salt solution tracer experiments were conducted to monitor the rate of water

186 transfer through the columns (assuming NaCl is a conserved tracer that does not interact with the
 187 solid-phase materials). The NaCl solution was passed into the system for 10 minutes and then
 188 replaced with tap water. The change in conductivity was measured over time using a hand-held
 189 electronic conductivity meter to produce NaCl (tracer) breakthrough curves. Results show good
 190 column flow consistencies similar to the volumetric flow measurements and both data sets are
 191 described in detail in Sections S1 and S2. The system was rigorously tested and checked for leaks
 192 during both the pre-conditioning and testing phases.



193
 194 *Figure 1: A. Schematic representation of the experimental setup. B. Theoretical model of the*
 195 *experiments indicating sorption and desorption phases and column termination points for solid*
 196 *phase analyses (2 columns terminated at 50 % breakthrough, 3 columns terminated at ≈equilibrium,*
 197 *and the final 3 columns terminated after desorption; end of experiment). C. Representation of the*
 198 *zones of mass transfer of Hg during the sorption phase (“saturated zone” refers to solid-phase in*
 199 *that zone reaching its equilibrium uptake capacity for Hg at the experimental solution*
 200 *concentration). The dark area describes the rising front of mercury. D. Allocation of column sections*
 201 *(≈15 mL in each section) for solid-phase analyses (“Bottom” is the solution entry point).*

202 10 mL of eluate was allowed to flow off into a waste vessel before 5 mL of sample was collected for
 203 analysis (this applied to all analyses). The liquid-phase was sampled for THg concentrations
 204 consistently throughout the experiments: 38x in EXP1 (10x up to ≈50% breakthrough – columns
 205 C1.1-C1.8; 11x between ≈50% breakthrough and ≈equilibrium – columns C1.1-C1.6; and 17x during
 206 desorption – columns C1.1-C1.3) and 35x in EXP2 (8x up to ≈50% breakthrough – columns C2.1-C2.8;
 207 16x between ≈50% and ≈100% breakthrough – columns C2.1-C2.3 and C2.6-C2.8; and 11x during

208 desorption – columns C2.1-C2.3). Liquid-phase speciation samples were collected 8x at ≈25%, 50%,
209 75% breakthrough, and ≈equilibrium, at the end of the equilibrium (immediately before stock
210 solution was changed to tap water), and ≈0% (immediately after stock solution was changed to tap
211 water), 50% and at the end of desorption for both experiments. Liquid-phase stable isotope samples
212 were collected only from columns C2.1-C2.3 in EXP2 9x in total. Collections were similar to liquid-
213 phase speciation sampling points with an additional collection during the sorption stage of the
214 experiment. After termination, solid-phase materials were analysed for THg concentrations, Hg
215 species, and Hg stable isotopes. In summary, C1.7 and C1.8 and C2.4 and C2.5 were sacrificed at
216 ≈50% breakthrough; C1.4-C1.6 and C2.6-C2.8 after equilibrium (≈100% breakthrough); while C1.1-
217 C1.3 and C2.1-C2.3 went through to the end of desorption.

218 2.2 Analyses

219 2.2.1 Liquid-phase THg and speciation analyses

220 Eluate samples for THg and Hg stable isotope analyses were immediately stabilized by adding 1% by
221 volume of 0.2 M bromine monochloride (BrCl) prepared according to Bloom et al. (2003). In order
222 to break up all of the organically bound mercury in the liquid, a reaction time of the BrCl of 24-hours
223 is recommended (US EPA method 1631, 2002). However, with little OM (Table 1), we assessed
224 sample THg analysis only 1-hour after BrCl addition and there was no impact on sample recovery
225 (Table S1.2). Immediately prior to analysis, hydroxylamine hydrochloride (NH₂OH·HCl) was added to
226 neutralize the BrCl followed by addition of tin(II) chloride (SnCl₂) solution as the Hg reducing agent.

227 Liquid-phase speciation analyses followed the same methods described elsewhere (Bollen et al,
228 2008; Richard et al., 2016b; McLagan et al., 2022). We describe this method as a complementary,
229 semi-quantitative analytical tool and produces four distinct “fractions” of the total pool of liquid-
230 phase Hg: (i) elemental Hg (Hg(0)) (purged from untreated eluate sample), (ii) dissolved inorganic
231 Hg(II) termed Hg(II)A; (purged after reduction with SnCl₂ treatment; e.g. HgCl₂); (iii) DOM-bound
232 Hg(II) termed Hg(II)B (purged after BrCl and SnCl₂ treatment), and (iv) particulate Hg termed Hg(II)P
233 (difference between THg concentrations in filtered and total unfiltered eluate samples). Both
234 concentration and speciation results were measured using a cold-vapor atomic absorbance
235 spectrometer (CV-AAS) (Hg-254 NE, Seefeldler Messtechnik GmbH, Germany) according to DIN
236 method 1483 (2007) and USEPA method 1631 (2002). Confidence in liquid phase Hg(0)
237 concentrations is higher than for other species, as these result from purging untreated/unstabilised
238 samples of Hg(0) with nitrogen gas directly into the CV-AAS; all Hg(0) samples were analysed within
239 30 mins of sample collection.

240 2.2.2 Solid-phase THg and speciation analyses

241 After individual columns were sacrificed for solid-phase analyses, the ends of the columns were
242 sealed to prevent the columns from draining and stored in the same upright position as the
243 experimental setup (Figure 1) to prevent further disturbance. Columns were cut into sections (Figure
244 1D), homogenised and subset within 1 week of the end of the experiments and stored at 4 °C in
245 brown (opaque) falcon tubes until digestions or analyses. All analyses were performed on wet
246 samples to minimise any potential losses of Hg(0). The moisture content of solid-phase samples was
247 determined on separate aliquots for each column by difference after drying at 35 °C and was 23 ±
248 2% (*n* = 48) (Section S8).

249 THg and Hg stable isotope analyses were cold digested in modified aqua regia following the methods
250 described in McLagan et al. (2022) (8 mL HCl, 3 mL HNO₃, and 1mL BrCl). Analyses of THg
251 concentrations from the digestion extracts were determined using CV-AAS following DIN method
252 1483 and USEPA method 1631. Results are reported on a dry weight basis and moisture content was
253 determined by difference after baking at 105 °C using aliquots of the solid-phase sample (Section
254 S8). Due to the low concentrations in the original solid-phase aquifer materials, THg concentrations
255 were measured with a DMA80 (Milestone SCI) via thermal decomposition, amalgamation, and AAS
256 (Table 1).

257 Speciation analyses were performed by pyrolytic thermal desorption (PTD), which continually
258 measures Hg at 254 nm within an AAS detector that is connected to a sample combustion furnace
259 that heats samples from room temperature to 650°C a 1°C per minute in a stream of N₂ gas. This
260 method is described in detail by Biester and Scholz (1996). The sample release curves were
261 compared to the release curves for a series of Hg reference materials (Hg(0), HgCl₂, Hg₂Cl₂ (calomel),
262 cinnabar: α-HgS, metacinnabar: β-HgS, and Hg²⁺-sulphate: HgSO₄) in silicon dioxide (SiO₂) matrix
263 (see Section S9 for reference material curves) to qualitatively assess the species or “fractions” of Hg
264 present in the samples.

265 2.2.3 Liquid- and solid-phase Hg stable isotope analyses

266 Samples for stable Hg isotope analyses included stabilized liquid-phase eluate samples and solid-
267 phase aqua-regia extracts diluted with deionised water (18.2 MΩ cm). Liquid-phase samples were
268 collected in 15 mL polypropylene tubes and stabilized with BrCl to reach 1% of the sampled volume.
269 Analyses were made using a Nu Plasma II (Nu Instruments) multicollector inductively coupled
270 plasma mass spectrometer (MC-ICP-MS) with a cold-vapor generator (HGX-200; Teledyne Cetac)
271 that allows direct addition of Hg(0) into MC-ICP-MS plasma by reducing all Hg in samples with SnCl₂.
272 The isotope ratios were determined relative to NIST-3133 (National Institute of Standards and
273 Technology; NIST) using the standard bracketing approach and corrected for mass-bias using
274 thallium (Tl) doping from NIST-997 (NIST) introduced using an Aridus-2 desolvating nebulizer
275 (Teledyne CETAC). MDF was assessed by variation in δ²⁰²Hg, while Δ¹⁹⁹Hg, Δ²⁰⁰Hg, Δ²⁰¹Hg, and
276 Δ²⁰⁴Hg were used to assess MIF of odd and even isotopes) (see Grigg et al., 2018; McLagan et al.,
277 2022 for method details).

278 2.2.4 Complementary analyses

279 Metal cations in the solid- and liquid-phases were measured with inductively coupled plasma optical
280 emission spectrometry (ICP-OES; Varian 715-ES; Agilent Technologies Inc.). Solid-phase total carbon
281 (TC), total organic carbon (TOC), and total inorganic carbon (TIC; dissolved by hydrochloric acid)
282 were measured by infra-red detection of CO₂ released (DIMA 1000NT; Dimatec, Germany).
283 Dissolved organic carbon of stock solution and eluate was measured with a carbon/nitrogen
284 analyser (Multi N / C 2100; Analytic Jena) (see Section S2). Liquid-phase dissolved oxygen content,
285 redox potential, electrical conductivity, and pH were measured by handheld probes.

286 2.2.5 Retardation (R_D) and sorption/partitioning/distribution (K_D) coefficient calculations

287 The retardation coefficient (R_D) is essentially the ratio of the velocity of the water front (v_w) and
288 velocity of the Hg front delayed by sorption processes (v_{Hg}) moving through the columns (Equation
289 1). Since the path of the the soluble pollutant (Hg) and water are the same, transport time can be
290 determined based on the time it takes the fronts to pass through the columns (t_{Hg} and t_w,

291 respectively). NaCl breakthrough curve was used as a proxy for water based on the assumption it is
292 a conservative tracer. t_{Hg} and t_w are given when the respective ratios of the NaCl and THg
293 concentrations in the eluate is equal to half the input concentration (stock solution; $C_{eluate} / C_{initial} =$
294 0.5) (Patterson et al., 1993; Reichert, 1991; Schnaar and Brusseau, 2013).

$$295 \quad R_D = v_w / v_{Hg} = t_w / t_{Hg} \quad \text{Equation 1}$$

296 R_D is related to the sorption or partitioning or distribution coefficient (K_D ; mL g⁻¹) according to
297 Equation 2 and Equation 3 (USEPA, 2004):

$$298 \quad R_D = 1 + (\rho_b / n_e) K_D \quad \text{Equation 2}$$

$$299 \quad K_D = (R_D - 1) (n_e / \rho_b) \quad \text{Equation 3}$$

300 Where, n_e is the effective porosity (EXP1: 0.470 ± 0.008 , $n = 3$; EXP2: 0.459 ± 0.004 , $n = 3$; assumed
301 to be equal to total porosity), which is the ratio of the column pore volume (EXP1: 23.3 ± 0.5 mL, n
302 = 3; EXP1: 22.5 ± 0.1 mL, $n = 3$) to the total volume of the solid-phase materials of the columns (EXP1:
303 49.7 ± 0.3 mL, $n = 3$; EXP2: 49.0 ± 0.5 mL, $n = 3$). R_D could only be calculated for columns that went
304 to equilibrium and desorption (not 50% breakthrough), n_e was calculated for columns that went
305 through desorption (C1.1-C1.3 and C2.1-C2.3); and hence, K_D was only calculated for these columns.
306 Note, the pore volumes reported above are the data used when reporting the number of pore
307 volumes.

308 2.3 Quality Assurance and quality control (QAQC)

309 For liquid-phase analyses, a 140.8 ng L^{-1} Hg(II) stock solution (Sigma Aldrich) was measured
310 throughout the analyses and recovery was $99 \pm 5\%$ ($n = 250$). For solid-phase analyses, Chinese Soil
311 (NCS DC73030; Chinese National Analysis Centre for Iron and Steel) was measured and recovery was
312 $101 \pm 6\%$ ($n = 16$). The accuracy and precision of Hg stable isotope measurements was assessed
313 using the “in-house” *ETH Fluka* standard. Mean values across the measurement sessions were:
314 $\delta^{202}\text{Hg} = -1.42 \pm 0.08 \text{ ‰}$; $\Delta^{199}\text{Hg} = 0.08 \pm 0.02 \text{ ‰}$; $\Delta^{200}\text{Hg} = 0.02 \pm 0.02 \text{ ‰}$; $\Delta^{201}\text{Hg} = 0.03 \pm 0.03 \text{ ‰}$;
315 $\Delta^{204}\text{Hg} = -0.01 \pm 0.06 \text{ ‰}$ ($n = 26$; all uncertainty values are reported as 2SD). All uncertainties are
316 1SD, unless otherwise reported (i.e., 2SD used to report Hg stable isotope analysis uncertainty).
317 These values are within the range of other studies (i.e., Obrist et al., 2017; Goix et al., 2019; McLagan
318 et al., 2022). Theoretical solid-phase THg concentration (compared to measured THg
319 concentrations) are determined via mass balance of liquid-phase THg concentrations of stock
320 solution and eluate and the volume of stock solution applied to the columns. All statistical tests and
321 sorption fitting comparisons were performed in OriginPro 2018 (Origin Lab Corporation).

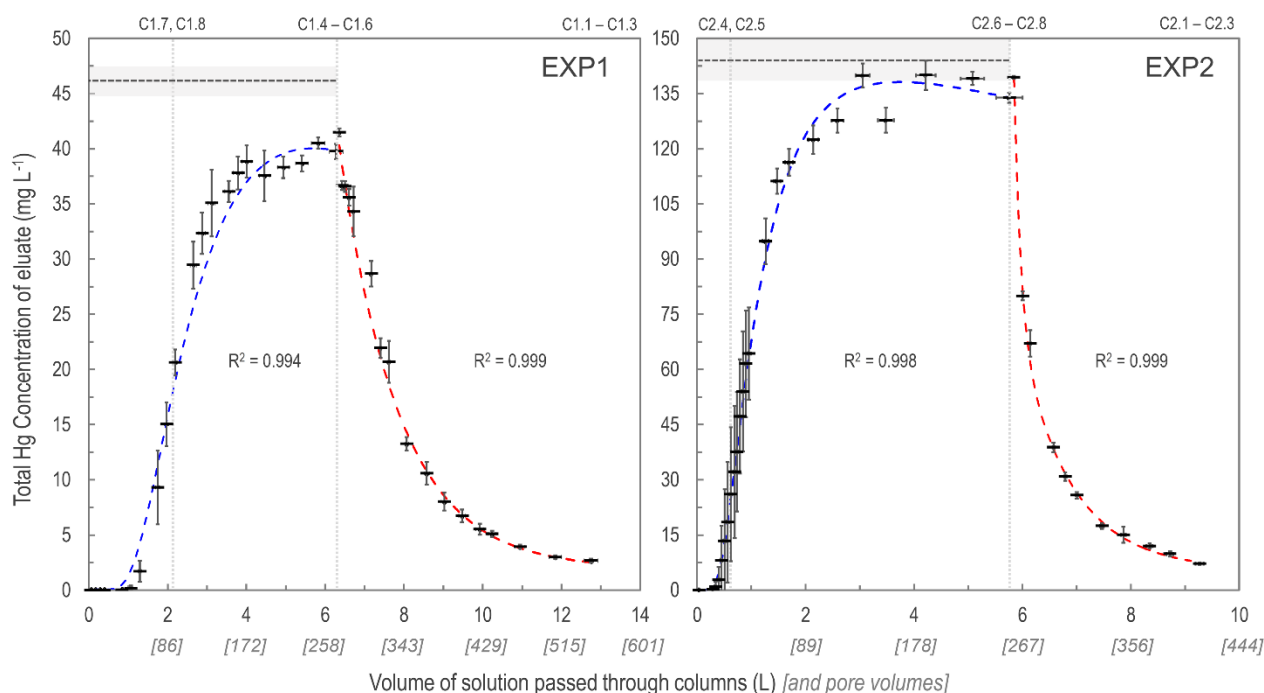
322 3 Results and discussion

323 3.1 Sorption and desorption behaviour of mercury in column experiments

324 3.1.1 Sorption

325 As expected, the uptake of the HgCl₂ solution to the solid phase aquifer materials followed an *S-*
326 *shaped* breakthrough curve best described by a Freundlich function (Figure 2; note these are
327 empirically fitted functions). Initially, >99.9% of the Hg in solution was sorbed to the solid phase
328 materials and 1.0-1.3 L (43 – 55 pore volumes) and 0.3-0.45 L (13 – 16 pore volumes), in EXP1 and
329 EXP2, respectively, was required to reach eluate THg concentrations equivalent to 1% of stock

330 solution (Section S5). This was followed by a phase of rapid increase in the eluate concentrations
 331 (decreasing fraction of the Hg in solution sorbing to the solid-phase). Finally, the increase in eluate
 332 THg concentration slowed as it approached the upper asymptotic bound of the original stock
 333 solution concentration in each experiment and equilibrium of Hg fluxes between the solid- and
 334 liquid-phases was approached/reached. EXP1 likely did not completely reach a stable equilibrium
 335 point (eluate concentration was at $\approx 91\%$ of stock solution concentration when the stock solution
 336 was changed to water), and more time/volume of solution was required. This would have required
 337 creation of more stock solution; instead, green chemistry prevailed, and the choice was made to
 338 move onto the desorption phase with consideration of the higher concentration (faster) follow-up
 339 EXP2.



340

341 *Figure 2: Total Hg concentration eluate breakthrough curves for low (EXP1; left panel) and high*
 342 *(EXP2; right panel) concentration stock solution experiments. Horizontal dashed lines (mean) and*
 343 *shaded area (1SD) indicate the original stock solution concentrations in each experiment and vertical*
 344 *dotted lines indicate column removal points (column IDs above panels indicate which columns were*
 345 *removed). Uncertainty in the x-axis relates to the differing volumes passed through individual*
 346 *columns at each sampling period. Sorption curves were fitted with Freundlich functions (blue dashed*
 347 *lines), and desorption curves were fitted with exponential decay functions (red dashed lines). These*
 348 *functions were empirically (not mechanistically) fitted to the data as these plots are not sorption*
 349 *isotherms (see Section S6 for details of fitting functions).*

350 This S-shaped sorption behaviour was similar to the one other detailed study on Hg sorption in
 351 natural soils with sufficient liquid-phase sampling frequency to create column breakthrough curves
 352 on OM-rich (9.4 – 24.7% OM) Amazonian soils and similar stock solution concentrations (60 – 120
 353 mg L⁻¹; Miretzky et al., 2005). Semi-quantitative liquid-phase Hg speciation analyses confirm that
 354 the majority of Hg was dissolved inorganic Hg(II) (EXP1: $83 \pm 6\%$; EXP2: $77 \pm 8\%$), a fraction of which
 355 will be soluble HgCl₂ (species used to generate stock solution), but also fractions of hydrolysed
 356 species (i.e., HgClOH, Hg(OH)₂, [HgCl₃]⁻) formed in solution at pH in the observed range (7.7 – 8.1)
 357 of these experiments (Delnomdedieu et al., 1992; Gunneriusson and Sjöberg, 1992; Kim et al., 2004;
 358 see also Section S10 for theoretical Hg speciation results using Visual MINTEQ v3.1). These liquid-

359 phase Hg speciation results are similar to those reported for groundwater samples previously
360 collected at the contaminated site where these materials were extracted from (Bollen et al., 2008;
361 Richard et al., 2016a; McLagan et al., 2022).

362 Despite the very low OM content (Table 1) within these solid-phase aquifer materials, the
363 equilibrium uptake capacity was very high in both experiments. These concentrations were
364 determined both (i) analytically by solid-phase THg analyses, and (ii) theoretically, based on the
365 inverse of the breakthrough curve integral: the area above the curve and below the stock solution
366 concentration. This has been referred to as “holdup” (H ; mg of Hg), (Van Genuchten and Parker,
367 1984) and is described in Equation 4:

$$368 \quad H = [C_0 V_f - \int C_e dV] \quad \text{Equation 4}$$

369 Where, C_e is the eluate THg concentration (mg L^{-1}), C_0 is the stock solution THg concentration (mg
370 L^{-1}), and V_f is the accumulated solution volume that has passed through the columns at the point
371 they were removed (L). Theoretical concentrations reached $1880 \pm 20 \text{ mg kg}^{-1}$ in EXP1 and $2810 \pm$
372 40 mg kg^{-1} in EXP2 (Table 2; Section S3). These data are directly comparable, and indeed within the
373 same range as the theoretical solid-phase concentrations calculated by Miretzky et al. (2005) for the
374 OM-rich Amazonian soils (THg concentrations: $950 - 3960 \text{ mg kg}^{-1}$). The elevated Hg sorption
375 observed by Miretzky et al. (2005) is to be expected due to the affinity of Hg for OM (e.g., Yin et al.,
376 1996; Jiskra et al., 2015; Manceau and Nagy, 2019). Nonetheless, Miretzky et al. (2005) found their
377 calculated solid-phase THg concentrations at equilibrium (sorptive capacity of the soils) were
378 greater when OM% + clay% was considered rather than OM% alone was considered (Miretzky et al.,
379 2005), which highlights the potential role clay (and oxide) minerals can play in Hg sorption to solid-
380 phase soil or aquifer materials.

381 Hg sorption to OM has been observed to increase at lower pH (Andersson, 1979; Yin et al., 1996).
382 However, the opposite has been reported for sorption of Hg to clay minerals: in neutral and slightly
383 basic soils, the sorption capacity is controlled by the mineral components (Andersson, 1979;
384 Schuster, 1991; Gabriel and Williamson, 2004). Indeed, the pH range of the eluate and stock solution
385 (pH range: 7.7 – 8.1) present ideal conditions for Hg sorption to clay minerals and Fe and Mn
386 (oxy)hydroxide minerals. Hg sorption to these inorganic minerals becomes more likely in our
387 experiments considering the very low OM content of the solid-phase materials (Table 1). Haitzer et
388 al. (2002) estimated that at ratios of THg-to-OM above $1 \mu\text{g}$ of Hg per mg of OM the strong thiol-
389 group bonding sites for Hg within OM are saturated. Based on the TOC data of these solid-phase
390 materials (assuming 0.16% TOC = 0.32 % OM), there would be 224 mg of OM within a column. To
391 surpass the ratio of $1 \mu\text{g}$ of Hg per mg of OM, only 4.9 and 1.6 mL of stock solution or 0.21 and 0.07
392 pore volumes in EXP1 and EXP2, respectively, would need to be added to the columns to saturate
393 the strong thiol-group binding sites with Hg. Considering that Hg breakthrough occurred only after
394 about 50 and 15 pore volumes in EXP1 and EXP2, respectively, it can be assumed that not only the
395 strong Hg-binding thiol-groups but also the other less strong Hg-binding functional groups (e.g.,
396 carboxyl groups) of the small OM pool in the columns were fully saturated early in the experiments.
397 Hence, solid-phase sorption of Hg within these experiments was dominated by interactions with
398 inorganic minerals. The role of such inorganic minerals was also highlighted in one of the few studies
399 that exist examining Hg transport and fate in aquifers (Lamborg et al., 2013).

400 *Table 2: Theoretical (liquid-phase THg mass-balance) and measured solid-phase THg concentrations*
 401 *and recovery of the measured-to-expected (theoretical) concentrations for each the columns in EXP1*
 402 *and EXP2.*

Experiment 1 (EXP1; $46.1 \pm 1.1 \text{ mg L}^{-1}$)					Experiment 2 (EXP2; $144 \pm 6 \text{ mg L}^{-1}$)				
Column	Stage	Theoretical Hg conc. (mg kg^{-1})	Measured Hg conc. (mg kg^{-1})	Recovery	Column	Stage	Theoretical Hg conc. (mg kg^{-1})	Measured Hg conc. (mg kg^{-1})	Recovery
C1.1	Desorption	820	722 ± 91	88.0%	C2.1	Desorption	1360	1060 ± 230	78.3%
C1.2	Desorption	890	877 ± 206	98.6%	C2.2	Desorption	1300	786 ± 390	60.2%
C1.3	Desorption	847	835 ± 120	98.6%	C2.3	Desorption	1490	1050 ± 57	70.1%
C1.4	Equilibrium	1870	1470 ± 221	78.5%	C2.4	50% breakthrough	1030	785 ± 220	76.1%
C1.5	Equilibrium	1910	1630 ± 286	85.1%	C2.5	50% breakthrough	1140	702 ± 330	61.4%
C1.6	Equilibrium	1870	1440 ± 92	77.1%	C2.6	Equilibrium	2770	2380 ± 452	86.1%
C1.7	50% breakthrough	1320	1470 ± 384	111.3%	C2.7	Equilibrium	2850	2320 ± 388	81.2%
C1.8	50% breakthrough	1300	960 ± 524	73.6%	C2.8	Equilibrium	2820	2260 ± 272	79.8%

403

404 Measured THg concentrations were typically lower than the theoretical calculated values (Table 2)
 405 and contaminant masses can be difficult to balance in contaminant batch and column experiments
 406 (Van Genuchten and Parker, 1984; Hebig et al., 2014). This is of particular concern for a contaminant
 407 such as Hg whose stability and contamination issues have been widely studied due to the capacity
 408 of different Hg species to sorb to and diffuse through plastic polymers (at differing rates) (Hall et al.,
 409 2002; Parker and Bloom, 2005; Hammerschmidt et al., 2011). Loss of a fraction of the THg in solution
 410 to/through tubing and the walls of the column is likely contributing to the lower recovery in some
 411 of these samples. Other factors that could be contributing to the differences between the
 412 theoretical and measured concentrations are heterogeneity of the solid-phase and solid-phase
 413 sample extraction (particularly during movement of the Hg mass transfer front), loss of Hg from
 414 solid-phase before sample extraction and analyses (particularly for volatile Hg(0); Parker and Bloom,
 415 2005), and inherent analytical uncertainties. The heterogeneity of the materials is emphasized by
 416 the absence of trends in THg concentrations within the sections of the columns, even for the
 417 columns undergoing movement of the mass transfer zone (see Section S8). Unfortunately, Miretzky
 418 et al. (2005) did not provide total sampling volumes for their experiments and no assessment of
 419 measured THg recoveries was (or can be) made for direct comparison to our recovery data.

420 3.1.2 Desorption

421 The desorption phase of both EXP1 and EXP2 followed an exponential decay model; results confirm
 422 that sorption is (partially) reversible and initially rapid (Figure 2). After the stock solution was
 423 switched to water for the desorption phase, the eluate solution reached <50% of the stock solution
 424 THg concentration with additions of $\approx 1 \text{ L}$ (≈ 43 pore volumes) and $\approx 0.5 \text{ L}$ (≈ 22 pore volumes) of
 425 solution in EXP1 and EXP2, respectively (Figure 2). At the termination of the experiments eluate THg
 426 concentrations dropped to <10% of the original stock solution (Figure 2). While it is evident that
 427 more Hg would have been released if desorption was permitted to proceed further (terminated due
 428 to time and to prevent excess contaminated waste solution), measured data indicated that $46 \pm 6\%$
 429 (Theoretical: $55 \pm 2\%$) in EXP1 and $58 \pm 10\%$ (Theoretical: $51 \pm 4\%$) in EXP2 of THg could be extracted
 430 from the solid-phase materials before the experiments were terminated. Evidence from the
 431 contaminated aquifer where these solid-phase materials were extracted suggest that the retention
 432 of a fraction of this Hg within the solid-phase materials is long-term (Bollen et al., 2008; McLagan et

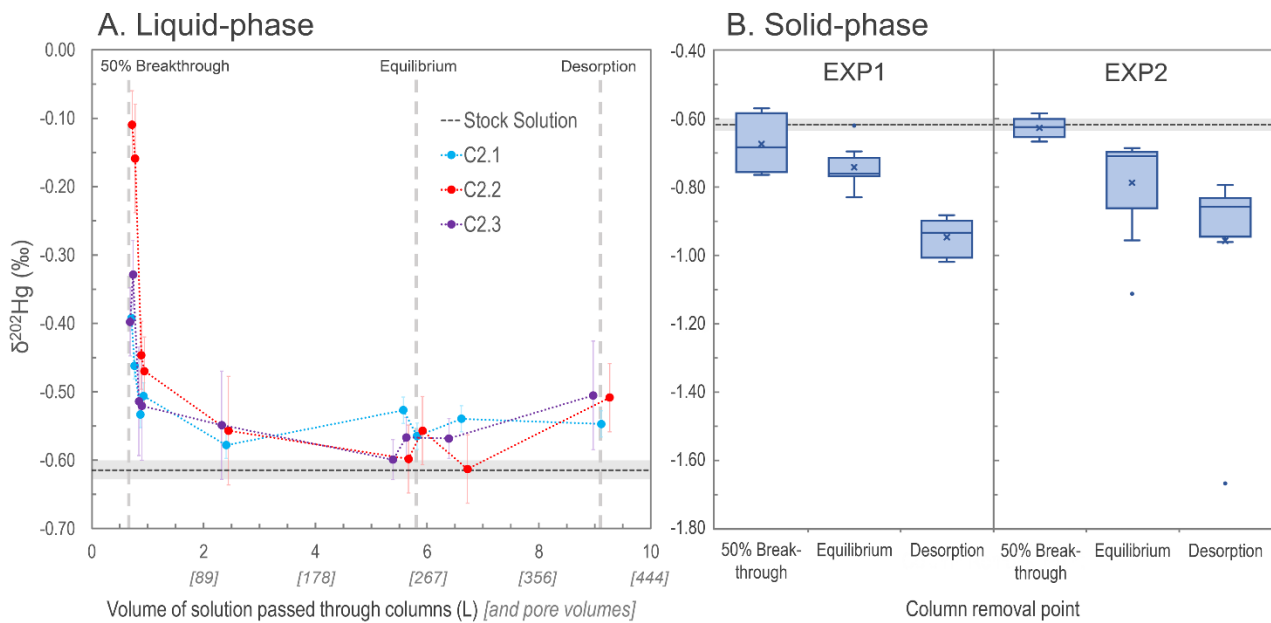
433 al., 2022). McLagan et al. (2022) report that elevated solid- (up to 562 mg kg⁻¹) and liquid-phase (up
434 to 164 ± 75.4 µg L⁻¹) THg concentrations are still found at the site to the present day, more than 55
435 years since the industrial use of Hg (kyanisation) at the site ceased.

436 McLagan et al. (2022) associate this residual retention of Hg to the diffusion of Hg into the mineral
437 matrix or secondary transformation to a more stable (and less soluble) Hg(II) species (McLagan et
438 al., 2022). Previous work agrees that sorption and subsequent release of Hg to/from solid-phase
439 soils and solid-phase materials is likely controlled by multiple processes (Yin et al., 1997; Bradl, 2004;
440 Reis et al., 2016). The more easily extractable Hg is likely to be associated with Fe and Mn
441 (oxy)hydroxide, and clay minerals through outer-sphere complexes that form through cation
442 exchange and electrostatic intermolecular forces (Bradl, 2004; Reis et al., 2016). Over time, some of
443 the Hg associated through these weaker surface interactions will diffuse into the matrix and/or form
444 inner-sphere complexes, processes that both slow the release of the sorbed Hg (Bradl, 2004; Reis et
445 al., 2016). Similar results were observed by Miretzky et al. (2005) in the OM rich Amazonian soil
446 columns with 27 - 38% of Hg sorbed to the solid-phase materials being rapidly redissolved in the
447 initial desorption phase. However, the soils with higher OM content showed stronger hysteresis and
448 considerably less Hg was released during the second phase of desorption (Miretzky et al., 2005) than
449 in our low OM solid-phase materials suggesting stronger interactions of inner-sphere complexed Hg
450 with OM; results supported by work done in other studies examining Hg sorption to solid-phase
451 materials (Yin et al., 1996; Reis et al., 2016).

452 3.1.3 Insights from stable Hg isotopes

453 Variations in δ²⁰²Hg values, describing MDF of Hg isotopes, were observed in both the liquid- and
454 solid-phase across the experiments (Figure 3; Section S7; Section S8). During the initial phase of the
455 experiments (before eluate breakthrough), transfer of Hg from the applied stock solution
456 (δ²⁰²Hg: -0.61 ± 0.01‰ relative to NIST-3133, 1SD; n = 3) to the solid-phase materials is complete.
457 When there is complete transfer of a “pool” of Hg from reactants to products there is complete
458 transfer of stable isotopes; and hence no fractionation can be observed.

459 Once Hg begins to breakthrough the columns, the eluate is initially enriched in heavy isotopes
460 associated with the preferential transfer (sorption) of lighter isotopes to the solid-phase materials
461 (Jiskra et al., 2012; Wiederhold, 2015) with heavier isotopes retained in solution (passed into the
462 eluate). In all three of the EXP2 columns examined for stable isotopes in the liquid-phase, the first
463 two liquid-phase stable isotope samples (sampled just after ≈50% breakthrough column removals)
464 had more positive δ²⁰²Hg values than the remaining liquid-phase samples (Figure 3). However, it is
465 also apparent that at ≈50% breakthrough, there was little MDF imparted on the solid-phase
466 materials compared to the stock solution (Figure 3). This ostensibly contrasting finding (observable
467 positive MDF in the liquid-phase and little negative MDF in the solid-phase) can be explained by the
468 proportion of Hg transferred to the solid-phase of the total mass added in solution. At the 50%
469 breakthrough column removal, the proportion of Hg sorbed by the columns was 95.4 and 90.4%,
470 respectively for C1.7 and C1.8 (EXP1) and 83.8 and 88.5%, respectively for C2.4 and C2.5 (EXP2;
471 based on theoretical calculations). The majority of this sorption occurred during the complete (or
472 near-complete) transfer of isotopes before (or just after) eluate breakthrough. Hence, the MDF that
473 began to occur after breakthrough (observable in the early liquid-phase eluate samples) had little
474 influence on the Hg stable isotope ratios of the solid-phase materials of columns removed at the
475 ≈50% breakthrough point.



476

477 *Figure 3: Development of liquid-phase $\delta^{202}\text{Hg}$ values for columns C2.1 – C2.3 measured at nine*
 478 *intervals during EXP2 (Panel A). Box plots of solid-phase $\delta^{202}\text{Hg}$ values measured in both EXP1 and*
 479 *EXP2 (“x” denotes mean values, dots denote outliers) (Panel B). In both panels, the grey dash line*
 480 *represents the mean $\delta^{202}\text{Hg}$ value (light grey rectangle: 1SD) measured for the stock solution. Note,*
 481 *the vertical grey dashed lines indicating solid-phase column removal points in the left panel are only*
 482 *approximations as the liquid-phase stable isotope measurements were only made on columns C2.1–*
 483 *2.3 that proceeded until the end of desorption.*

484 This finding of limited MDF on solid phase materials at $\approx 50\%$ breakthrough is consistent with the
 485 $\delta^{202}\text{Hg}$ values observed within the column layers. The bottom layers of C1.7 ($\delta^{202}\text{Hg}$: $-0.76 \pm 0.07\%$)
 486 and C1.8 ($\delta^{202}\text{Hg}$: $-0.75 \pm 0.07\%$) in EXP1 were more negative than the stock solution, while the top
 487 layers ($\delta^{202}\text{Hg}$: $-0.57 \pm 0.15\%$ and $\delta^{202}\text{Hg}$: $-0.59 \pm 0.07\%$ for C1.7 and C1.8, respectively) were
 488 equivalent to the stock solution (Section S8). These data suggest observable MDF was beginning to
 489 occur in the part of the column exposed to the Hg front (bottom) for the longest. The same was not
 490 the case in EXP2 (no observable trend in $\delta^{202}\text{Hg}$ between layers; Section S8). We attribute this to the
 491 more elevated THg concentrations and faster movement of the Hg front moving through the
 492 columns (see Table 3 below) in EXP2 overwhelming the layering MDF observed in EXP1.

493 As sorption progresses to equilibrium, we observe a negative shift in the eluate $\delta^{202}\text{Hg}$ value of all
 494 three columns falling in the range of ≈ -0.6 to -0.5% , which is slightly more positive than the stock
 495 solution ($\delta^{202}\text{Hg}$: $-0.61 \pm 0.01\%$ 1SD; $\pm 0.08\%$ analytical 2SD; Figure 3). During this transition in the
 496 Hg uptake process the net effect is that most, and then essentially all, Hg input from the stock
 497 solution is passing through the columns and into the eluate and any kinetic MDF occurring would
 498 be limited. Nonetheless, equilibrium-based isotope exchange would also drive lighter isotopes into
 499 the solid-phase materials (Wiederhold et al., 2010; Jiskra et al., 2012; Wiederhold, 2015), which is
 500 the likely explanation for the liquid-phase $\delta^{202}\text{Hg}$ values remaining slightly more positive than the
 501 stock solution. While the impact of this MDF on the continuously flowing eluate is small when the
 502 system is at equilibrium, the effect of this equilibrium-based MDF on the solid-phase is more
 503 manifest as its effect is cumulative. Over time, more and more lighter isotopes preferentially sorb
 504 to the solid-phase; and hence, the mean $\delta^{202}\text{Hg}$ values of the solid-phase materials in EXP1
 505 ($\delta^{202}\text{Hg}$: $-0.74 \pm 0.06\%$ 1SD) and EXP2 ($\delta^{202}\text{Hg}$: $-0.79 \pm 0.15\%$ 1SD) at the end of the sorption

506 experiments (at or near column equilibrium) are more negative than the stock solution (and solid-
507 phase materials at $\approx 50\%$ breakthrough). Thus, we suggest equilibrium-based MDF (with some
508 potential for kinetic MDF contributions) to be the primary driver of the more negative $\delta^{202}\text{Hg}$ values
509 observed in the solid-phase materials at the end of the equilibrium-phase of the experiments. These
510 observations agree with the observed results of McLagan et al. (2022) sampled within the
511 contaminated aquifer adjacent to which these uncontaminated materials were derived.

512 At the end of the desorption phase, the solid-phase materials have undergone further MDF to more
513 negative $\delta^{202}\text{Hg}$ values (EXP1 $\delta^{202}\text{Hg}$: $-0.95 \pm 0.05\%$; EXP2 $\delta^{202}\text{Hg}$: $-0.96 \pm 0.27\%$ 1SD). Two of the
514 three columns monitored for liquid-phase stable isotopes at the end of desorption also show a slight
515 positive MDF shift and values for all three columns are slightly more positive ($\delta^{202}\text{Hg}$: -0.55 to -0.51
516 $\%$) than the stock solution (Figure 3). As discussed, desorption proceeds via a two-step mechanism:
517 a rapid initial desorption as easily exchangeable, outer-sphere complexed Hg is released, followed
518 by a slower phase of desorption as this easily exchangeable pool depletes. Broczka et al. (2019) and
519 McLagan et al. (2022) suggest that this easily exchangeable pool is enriched in heavier isotopes
520 compared to the fraction that diffuses into the mineral matrix or transforms to more stable, less
521 soluble Hg(II) species as these secondary processes favour lighter isotopes. Thus, removal of the
522 heavy isotope enriched, easily exchangeable pool of Hg is the likely driver of more negative $\delta^{202}\text{Hg}$
523 values in the solid-phase materials after desorption. While Demers et al. (2018) studied
524 predominantly surface water samples linked to Hg soil-groundwater contamination at a site in
525 Tennessee, USA (industrial use of Hg(0)), they did observe more positive $\delta^{202}\text{Hg}$ values with elevated
526 dissolved THg concentrations values in samples from the hyporheic zone associated with exfiltrating
527 groundwater from the contaminated areas. These data would agree with the more positive liquid-
528 phase $\delta^{202}\text{Hg}$ values observed in our study and by McLagan et al. (2022).

529 Variation in both odd- and even-isotope MIF was within the range of analytical uncertainties
530 (Section S7; Section S8). McLagan et al. (2022) did observe small variation in $\Delta^{199}\text{Hg}$ between solid-
531 and liquid-phases, which the authors suggest may be linked to MIF driven by dark abiotic reduction
532 of Hg(II) (Zheng and Hintelmann, 2010). However, it is unlikely that this process could manifest into
533 an observable change in $\Delta^{199}\text{Hg}$ considering the short duration of these experiments even if the
534 process could occur at all within these columns.

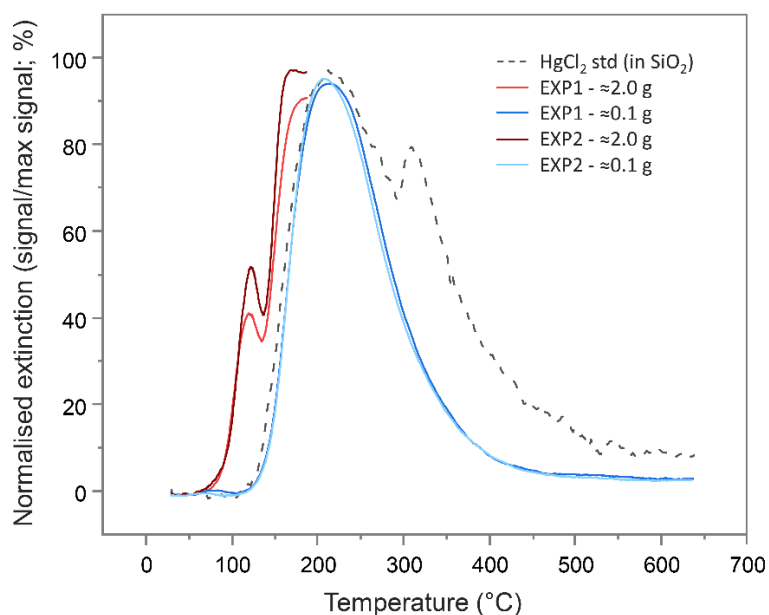
535 3.2 Is reduction of Hg(II) to Hg(0) occurring within the columns?

536 Reduction of Hg(II) to Hg(0) has been observed previously at this and other sites impacted by
537 kyanisation activities (Bollen et al., 2008; Richard et al., 2016a; 2016b; McLagan et al., 2022). In
538 these subsurface environments with low OM and very high THg concentrations, this secondary Hg(0)
539 production has been linked to abiotic, (hydr)oxide mineral surface catalysed reactions driven by
540 other redox active metals (Bollen et al., 2008; Richard et al., 2016a; 2016b; Schwab et al., 2023).
541 Since HgCl_2 solution was the only form of Hg applied in the column experiments, the presence of
542 Hg(0) in either the liquid- or solid-phases must be explained via reduction of Hg(II).

543 To examine the presence of Hg(0), PTD analyses were run on the (undried) solid-phase materials
544 from the columns after the sorption experiments. The PTD extinction curves showed little variation
545 across all sections of all columns from either experiment (see Section S9). All curves mimic the low
546 sample weight (≈ 0.1 g) mean extinction curves displayed in Figure 4 and are dominated by a single
547 peak with a maximum release of ≈ 225 °C, which aligns with the maximum extinction of the HgCl_2
548 standard in silicon dioxide (SiO_2). This supports the hypothesis of direct (outer-sphere) complexation

549 or electrostatic interaction of dissolved Hg(II) species to the mineral surfaces posited previously
550 (Bradl, 2004; Reis et al., 2016) and by McLagan et al. (2022). Nonetheless, these low sample weight
551 PTD curves were indicative of some qualitative evidence of very small peaks at <175 °C (Section S9);
552 peaks in this range are associated with Hg(0) (Biester and Scholz, 1996; McLagan et al., 2022). The
553 initial sample masses used in the PTD analyses were low (≈ 0.1 g) so as to not overwhelm the AAS
554 detector, release large amounts of gas-phase Hg(0), and potentially cause memory effects in future
555 analyses. Nevertheless, this would not occur if sample masses were increased (≈ 2.0 g) and the
556 temperature ramp stopped at ≈ 175 °C. When the solid-phase materials were analysed in this
557 manner, Hg(0) peaks were detected across all sections of all columns in both experiments (see
558 Section S9; Figure 4).

559 Additionally, detectable concentrations of Hg(0) were observed across all of the semi-quantitative
560 liquid-phase Hg speciation analyses and elevated above the Hg(0) concentrations measured in the
561 stock solution (Section S4). The observed liquid-phase fraction of Hg(0) was highest at the $\approx 25\%$
562 breakthrough sample collection point in EXP1 (0.7%) and EXP2 (0.1%) with the fraction being $\leq 0.1\%$
563 in all other samples (Section S4). While these data suggest that reduction of Hg(II) to Hg(0) begins
564 almost immediately after the introduction of the HgCl₂ solution, we link the declining proportion of
565 Hg(0) to the low solubility of Hg(0) ($\approx 50 \mu\text{g L}^{-1}$) (Skylberg, 2012; Brocza et al., 2019), which was
566 already reached at the $\approx 25\%$ breakthrough sample collection point in both experiments.



567

568 *Figure 4: Mean pyrolytic thermal desorption (PTD) extinction curves from solid-phase materials from*
569 *EXP1 and EXP2 assessed with two different sample masses. Analyses of the larger sample mass (≈ 2.0*
570 *g of material) were terminated when the temperature ramp reached ≈ 175 °C to prevent excessive*
571 *gas-phase Hg release and potential memory effects on the instrument.*

572 These measured Hg(0) fractions in solid- and liquid-phase analyses provide further direct evidence
573 of Hg(0) production under saturated, oxic conditions in low OM solid-phase materials. Hg(0)
574 production in these contaminated aquifers has been linked to the slower than expected horizontal
575 progress of the plume of Hg in the aquifer at the site where this contamination occurred (Bollen et
576 al., 2008; Richard et al., 2016a; 2016b; McLagan et al., 2022). While these data indicate that the
577 fraction of Hg(0) produced is relatively small, the volume of soil and aquifer materials in which this
578 process can occur is large. The contamination plume of the aquifer at the site where the solid phase

579 materials were removed from is ≈ 1000 m long and covers an area of $\approx 6 \times 10^4$ m² (Bollen et al., 2008;
 580 McLagan et al., 2022). If we assume conservative values for mean depth of contamination of 2 m
 581 (aquifer ≈ 3 -4 m depth; Bollen et al., 2008; McLagan et al., 2022), mean THg concentration of 2 mg
 582 kg⁻¹ (solid phase THg concentration of 2-162 mg kg⁻¹ along the contaminated aquifer; Bollen et al.,
 583 2008), the fraction of Hg(0) produced per day is 0.01 – 0.001% of the THg (based off 0.1% Hg(0) peak
 584 integration of total peak area of mean PTD curve from EXP2; see Section S9)), and the same bulk
 585 density and flow rates as in our experiments, we can produce a *back-of-the-envelope* estimate of
 586 the mass of Hg(0) produced and potentially lost from the aquifer to overlying soils. Based off these
 587 numbers, we estimate that 0.3 – 0.4 g of Hg(II) is transformed to Hg(0) each day within the aquifer
 588 of the contaminated site in southern Germany; over the course of one-year, this equates to the
 589 transformation ≈ 5 – 15 kg of Hg(II) to Hg(0). Even a relatively conservative estimate of the
 590 conversion (and potential loss) of this mass of Hg(II) in contaminated aquifers such as this provides
 591 strong evidence that the process of Hg(II) reduction plays a key role in limiting the transport of the
 592 10-20 tonnes of Hg that was added to this soil-groundwater system in the ≈ 120 years since industrial
 593 operations commenced.

594 3.3 Retardation (R_D) and sorption coefficient (K_D) calculations

595 As expected, R_D values were substantially greater than 1, confirming substantial interaction
 596 between the applied HgCl₂ solution and the solid-phase aquifer materials (Table 3). The difference
 597 in R_D and K_D values between EXP1 and EXP2 (Table 3) indicate stock solution concentration is a factor
 598 in the transport of mercury within these columns. The elevated stock solution concentrations may
 599 be undermining the assumption of equal accessibility to sorption sites (USEPA, 2004). However, the
 600 purpose of these experiments was to simulate the original contamination by the industrial (mis)use
 601 of HgCl₂ solution, and while we can only estimate original concentration of solution being
 602 transported through the soil-groundwater system, we do expect they were very high due to the
 603 extent (both in terms of elevated concentrations and longitudinal and transverse dispersion of the
 604 contamination plume) of contamination that remains and the very high concentration of the
 605 solution used in rot-prevention treatment of timber (Bollen et al., 2008; Richard et al., 2016a;
 606 McLagan et al., 2022). Considering the high concentrations of Hg that have been observed within
 607 this and other Hg contaminated aquifers (Katsenovich et al., 2010; Lamborg et al., 2013; Demers et
 608 al., 2018), it is critical that we do not isolate our study of Hg transport dynamics to low concentration
 609 experiments that meet assumptions for theoretical sorption (batch and column) experiments.

610 *Table 3: Calculated retardation (R_D) and sorption (K_D) coefficients for EXP1 and EXP2 (definitions are*
 611 *given in Section 2.2.5).*

EXP1					EXP2				
Column	t_w (min)	t_{Hg} (min)	R_D	K_D (mL g ⁻¹)	Column	t_w (min)	t_{Hg} (min)	R_D	K_D (mL g ⁻¹)
C1.1	48.9	3628	74.7	23.8	C2.1	43.0	1615	37.6	11.8
C1.2	41.0	3629	88.5	29.5	C2.2	38.2	1567	41.2	12.9
C1.3	50.0	3779	75.6	25.1	C2.3	45.8	1837	39.9	12.6
C1.4	49.5	3678	74.3	-	C2.6	41.0	1438	35.1	-
C1.5	44.0	3488	79.3	-	C2.7	44.1	1623	36.9	-
C1.6	47.8	3599	75.3	-	C2.8	37.5	1317	35.1	-
		Mean	77.9	26.1			Mean	38.4	12.4
		SD	5.5	3.0			SD	2.7	0.6

612

613 R_D values can be calculated from Miretzky et al. (2005) based on the inverse of their v/v_{water} value
614 and the mean of these derived R_D values is 48 ± 13 for the high OM Amazonian soils. This again
615 affirms the high sorptive capacity of our low OM solid-phase aquifer materials at these comparative
616 concentration HgCl_2 applications. Lamborg et al. (2013) calculated K_D values for a Hg contaminated
617 (from wastewater treatment) aquifer between 100 and 6300 mL g^{-1} ($\log K_D$: 2-3.8); yet calculations
618 had to assume liquid-phase concentrations from other studies. $\log K_D$ values calculated from soil
619 and sediment batch experiments typically range from ≈ 2 in lower OM materials (Akçay et al., 1996)
620 up to ≈ 6 in higher OM materials (Lyon et al., 1997). The logical next step is to utilise the measured
621 R_D and K_D data from our study to perform soil-groundwater modelling to better understand Hg
622 transport in this and other soil-groundwater systems as there are no previous estimates of R_D and
623 K_D values based on measured data for low OM solid-phase aquifer materials. The range of coefficient
624 values from ours and other studies described above relating to differing solid-phase properties,
625 input solution speciation, and assumptions used highlights the caution that should be made applying
626 these values to other systems as R_D and K_D values tend to be highly site specific (USEPA, 2004).

627 Acknowledgements

628 We would like to thank Adelina Călean and Petra Schmidt for their support and contributions in
629 terms of experimental setup and sample analyses (including A.C. travelling to Vienna for to assist
630 with isotope analyses). We also thank undergraduate students Jan Pietrucha, Jette Greiser, and
631 Katja Braun for helping with liquid-phase sample collection and analyses. We thank Stephan M.
632 Kraemer for supporting the Hg isotope analyses at the University of Vienna. We would also like to
633 acknowledge Thomas Schöndorf from HPC Environmental Consulting for providing the solid-phase
634 materials used in this study. Also thanks to Hans Esser for helping design the eight-column holding
635 rack used in the experiments. This research was funded by the German Science Foundation (DFG)
636 grant BI 734/17-1 to H.B. and the Austrian Science Fund (FWF) grant I-3489-N28 to J.W. D.S.M.
637 would like to thank for support provided through a National Sciences and Engineering Research
638 Council of Canada (NSERC) postdoctoral fellowship.

639 Author contributions

640 D.S.M., C.E., and H.B. designed the study and experiments with some feedback from other co-
641 authors, particularly J.-H.R during preliminary experiments. C.E. led all concentration and speciation
642 analyses with assistance from D.S.M. Isotope analyses were led by L.S. with assistance from J.W.
643 (and A.C. see above). This work was the basis for C.E.'s master's thesis, which was written in German.
644 The manuscript first draft was written by D.S.M. and all other authors provided feedback in building
645 the manuscript towards submission. Figures, tables, and SI were produced by D.S.M, C.E., and L.S.

646 References

- 647 Andersson, A.: Mercury in soil, In: The biochemistry of mercury in the environment, edited by:
648 Nriagu, J. O., Elsevier, Amsterdam, Holland, 79-112, ISBN: 0444801103, 1979.
- 649 Akçay, H., Kiliç, S. İ. B. E. L., and Karapire, C.: A comparative study on the sorption and desorption
650 of Hg, Th and U on clay, J. Radioanal. Nucl. Chem., 214, 51-66, <https://doi.org/10.1007/bf02165058>,
651 1996.
- 652 Avotins, P. V.: Adsorption and coprecipitation studies of mercury on hydrous iron oxide, Stanford
653 University, Stanford, USA, ISBN: 9798660526602, 1975.

654 Bergquist, B. A., and Blum, J. D.: Mass-dependent and-independent fractionation of Hg isotopes by
655 photoreduction in aquatic systems, *Science*, 318, 417-420,
656 <https://doi.org/10.1126/science.1148050>, 2007.

657 Bergquist, B. A., and Blum, J. D.: The odds and evens of mercury isotopes: applications of mass-
658 dependent and mass-independent isotope fractionation, *Elements*, 5, 353-357,
659 <https://doi.org/10.2113/gselements.5.6.353>, 2009.

660 Bloom, N. S., Preus, E., Katon, J., and Hiltner, M.: Selective extractions to assess the
661 biogeochemically relevant fractionation of inorganic mercury in sediments and soils, *Anal. Chim.*
662 *Acta*, 479, 233-248, [https://doi.org/10.1016/S0003-2670\(02\)01550-7](https://doi.org/10.1016/S0003-2670(02)01550-7), 2003.

663 Bollen, A., Wenke, A., and Biester, H.: Mercury speciation analyses in HgCl₂-contaminated soils and
664 groundwater—implications for risk assessment and remediation strategies, *Water Res.*, 42, 91-100,
665 <https://doi.org/10.1016/j.watres.2007.07.011>, 2008.

666 Brocza, F. M., Biester, H., Richard, J. H., Kraemer, S. M., and Wiederhold, J. G.: Mercury isotope
667 fractionation in the subsurface of a Hg(II) chloride-contaminated industrial legacy site, *Environ. Sci.*
668 *Technol.*, 53, 7296-7305, <https://doi.org/10.1021/acs.est.9b00619>, 2019.

669 Bradl, H. B.: Adsorption of heavy metal ions on soils and soils constituents, *J. Colloid Interf. Sci.*, 277,
670 1-18, <https://doi.org/10.1016/j.jcis.2004.04.005>, 2004.

671 Clarkson, T. W.: The toxicology of mercury, *Crit. Rev. Clinic. Lab. Sci.*, 34, 369-403,
672 <https://doi.org/10.3109/10408369708998098>, 1997.

673 Demers, J. D., Blum, J. D., Brooks, S. C., Donovan, P. M., Riscassi, A. L., Miller, C. L., Zheng, W. and
674 Gu, B.: Hg isotopes reveal in-stream processing and legacy inputs in East Fork Poplar Creek, Oak
675 Ridge, Tennessee, USA, *Environ. Sci. Process. Impacts*, 20, 686-707,
676 <https://doi.org/10.1039/C7EM00538E>, 2018.

677 DIN ISO: Method 11277: Soil quality—Determination of particle size distribution in mineral soil
678 material—Method by sieving and sedimentation, German Institute for Standardisation (Deutsches
679 Institut für Normung; DIN) International Organization for Standardization (ISO), Berlin, Germany,
680 2002.

681 DIN: Method 1483: Water quality - Determination of mercury - Method using atomic absorption
682 spectrometry, German Institute for Standardisation (Deutsches Institut für Normung; DIN), Berlin,
683 Germany, 2007.

684 DIN: 19528-01: Leaching of solid materials - Percolation method for the joint examination of the
685 leaching behaviour of organic and inorganic substances for materials with a particle size up to 32
686 mm - Basic characterization using a comprehensive column test and compliance test using a quick
687 column test, German Institute for Standardisation (Deutsches Institut für Normung; DIN), Berlin,
688 Germany, 2009.

689 Gabriel, M. C., and Williamson, D. G.: Principal biogeochemical factors affecting the speciation and
690 transport of mercury through the terrestrial environment, *Environ. Geochem. Health*, 26, 421-434,
691 <https://doi.org/10.1007/s10653-004-1308-0>, 2004.

692 Gettens, R. J., Feller, R. L., and Chase, W. T.: Vermilion and cinnabar. *Stud. Conserv.*, 17, 45-69,
693 <https://doi.org/10.1179/sic.1972.006>, 1972.

694 Goix, S., Maurice, L., Laffont, L., Rinaldo, R., Lagane, C., Chmeleff, J., Menges, J., Heimbürger, L.E.,
695 Maury-Brachet, R. and Sonke, J. E.: Quantifying the impacts of artisanal gold mining on a tropical
696 river system using mercury isotopes, *Chemosphere*, 219, 684-694,
697 <https://doi.org/10.1016/j.chemosphere.2018.12.036>, 2019.

698 Grigg, A. R., Kretzschmar, R., Gilli, R. S., and Wiederhold, J. G.: Mercury isotope signatures of digests
699 and sequential extracts from industrially contaminated soils and sediments, *Sci. Tot. Environ.*, 636,
700 1344-1354, <https://doi.org/10.1016/j.scitotenv.2018.04.261>, 2018.

701 Gu, B., Bian, Y., Miller, C. L., Dong, W., Jiang, X., and Liang, L.: Mercury reduction and complexation
702 by natural organic matter in anoxic environments, *Proceed. Nat. Acad. Sci.*, 108, 1479-1483,
703 <https://doi.org/10.1073/pnas.1008747108>, 2011.

704 Gunneriusson, L. and Sjöberg, S.: Surface complexation in the H⁺-goethite (α -FeOOH)-Hg (II)-
705 chloride system, *J. Colloid Interf. Sci.* 156, 121-128, <https://doi.org/10.1006/jcis.1993.1090>, 1993.

706 Haitzer, M., Aiken, G. R., and Ryan, J. N.: Binding of mercury (II) to dissolved organic matter: the role
707 of the mercury-to-DOM concentration ratio, *Environ. Sci. Technol.*, 36, 3564-3570,
708 <https://doi.org/10.1021/es025699i>, 2002.

709 Hall, G. E., Pelchat, J. C., Pelchat, P., and Vaive, J. E.: Sample collection, filtration and preservation
710 protocols for the determination of 'total dissolved' mercury in waters, *Analyst*, 127, 674-680,
711 <https://doi.org/10.1039/B110491H>, 2002.

712 Hammerschmidt, C. R., Bowman, K. L., Tabatchnick, M. D., and Lamborg, C. H.: Storage bottle
713 material and cleaning for determination of total mercury in seawater, *Limnol. Oceanogr.*
714 *Methods*, 9, 426-431, <https://doi.org/10.4319/lom.2011.9.426>, 2011.

715 Hebig, K. H., Nödler, K., Licha, T., and Scheytt, T. J.: Impact of materials used in lab and field
716 experiments on the recovery of organic micropollutants, *Sci. Tot. Environ.*, 473, 125-131,
717 <https://doi.org/10.1016/j.scitotenv.2013.12.004>, 2014.

718 Ho, T. L.: Hard soft acids bases (HSAB) principle and organic chemistry, *Chem. Rev.*, 75, 1-20,
719 <https://doi.org/10.1021/cr60293a001>, 1975.

720 Jiskra, M., Wiederhold, J. G., Bourdon, B., and Kretzschmar, R.: Solution speciation controls mercury
721 isotope fractionation of Hg(II) sorption to goethite. *Environ. Sci. Technol.*, 46, 6654-6662,
722 <https://doi.org/10.1021/es3008112>, 2012.

723 Jiskra, M., Wiederhold, J. G., Skyllberg, U., Kronberg, R. M., and Kretzschmar, R.: Source tracing of
724 natural organic matter bound mercury in boreal forest runoff with mercury stable isotopes, *Environ.*
725 *Sci. Process. Impacts*, 19, 1235-1248, <https://doi.org/10.1039/C7EM00245A>, 2017.

726 Katsenovich, Y., Tachiev, G., Fuentes, H. R., Roelant, D., and Henao, A.: A study of the mercury (II)
727 sorption and transport with Oak Ridge Reservation soil, *Waste Management Conference 2010*,
728 Phoenix, USA, <https://archivedproceedings.econference.io/wmsym/2010/pdfs/10222.pdf>, 2010.

729 Kim, C. S., Rytuba, J. J., and Brown Jr, G. E.: EXAFS study of mercury (II) sorption to Fe-and Al-(hydr)
730 oxides: II. Effects of chloride and sulfate, *J. Colloid Interf. Sci.*, 270, 9-20,
731 <https://doi.org/10.1016/j.jcis.2003.07.029>, 2004.

732 Kocman, D., Horvat, M., Pirrone, N., and Cinnirella, S.: Contribution of contaminated sites to the
733 global mercury budget, *Environ. Res.*, 125, 160-170, <https://doi.org/10.1016/j.envres.2012.12.011>,
734 2013.

735 Lamborg, C. H., Kent, D. B., Swarr, G. J., Munson, K. M., Kading, T., O'Connor, A. E., Fairchild, G. M.,
736 LeBlanc, D. R., and Wiatrowski, H. A.: Mercury speciation and mobilization in a wastewater-
737 contaminated groundwater plume, *Environ. Sci. Technol.*, 47, 13239-13249,
738 <https://doi.org/10.1021/es402441d>, 2013.

739 Leterme, B., Blanc, P., and Jacques, D.: A reactive transport model for mercury fate in soil—
740 application to different anthropogenic pollution sources, *Environ. Sci. Poll. Res.*, 21, 12279-12293,
741 <https://doi.org/10.1007/s11356-014-3135-x>, 2014.

742 Lewis, J., and Sjöström, J.: Optimizing the experimental design of soil columns in saturated and
743 unsaturated transport experiments, *J. Contam. Hydrol.*, 115, 1-13,
744 <https://doi.org/10.1016/j.jconhyd.2010.04.001>, 2010.

745 Lockwood, R. A., and Chen, K. Y.: Adsorption of mercury (II) by hydrous manganese oxides, *Environ.*
746 *Sci. Technol.*, 7, 1028-1034, <https://doi.org/10.1021/es60083a006>, 1973.

747 Llanos, W., Kocman, D., Higuera, P., and Horvat, M.: Mercury emission and dispersion models from
748 soils contaminated by cinnabar mining and metallurgy, *J. Environ. Monit.*, 13, 3460-3468,
749 <https://doi.org/10.1039/C1EM10694E>, 2011.

750 Lu, Y. F., Wu, Q., Yan, J. W., Shi, J. Z., Liu, J., and Shi, J. S.: Realgar, cinnabar and An-Gong-Niu-Huang
751 Wan are much less chronically nephrotoxic than common arsenicals and mercurial, *Exp. Biol.*
752 *Med.*, 236, 233-239, <https://doi.org/10.1258/ebm.2010.010247>, 2011.

753 Lyon, B. F., Ambrose, R., Rice, G., and Maxwell, C. J.: Calculation of soil-water and benthic sediment
754 partition coefficients for mercury, *Chemosphere*, 35, 791-808, [https://doi.org/10.1016/S0045-6535\(97\)00200-2](https://doi.org/10.1016/S0045-6535(97)00200-2), 1997.

756 Manceau, A., and Nagy, K. L.: Thiols in natural organic matter: Molecular forms, acidity, and
757 reactivity with mercury (II) from First-Principles calculations and high energy-resolution X-ray
758 absorption near-edge structure spectroscopy, *ACS Earth Space Chem.*, 3, 2795-2807,
759 <https://doi.org/10.1021/acsearthspacechem.9b00278>, 2019.

760 McLagan, D. S., Schwab, L., Wiederhold, J. G., Chen, L., Pietrucha, J., Kraemer, S. M., and Biester, H.:
761 Demystifying mercury geochemistry in contaminated soil-groundwater systems with
762 complementary mercury stable isotope, concentration, and speciation analyses, *Environ. Sci.*
763 *Process. Impacts*, 24, 1406-1429, <https://doi.org/10.1039/D1EM00368B>, 2022.

764 Miretzky, P., Bisinoti, M. C., & Jardim, W. F.: Sorption of mercury (II) in Amazon soils from column
765 studies, *Chemosphere*, 60, 1583-1589, <https://doi.org/10.1016/j.chemosphere.2005.02.050>, 2005.

766 Norrby, L. J.: Why is mercury liquid? Or, why do relativistic effects not get into chemistry
767 textbooks? *J. Chem. Ed.*, 68, 110, <https://doi.org/10.1021/ed068p110>, 1991.

768 Obrist, D., Agnan, Y., Jiskra, M., Olson, C. L., Colegrove, D. P., Hueber, J., Moore, C.W., Sonke, J.E.
769 and Helmig, D.: Tundra uptake of atmospheric elemental mercury drives Arctic mercury
770 pollution, *Nature*, 547, 201-204, <https://doi.org/10.1038/nature22997>, 2017.

771 Parker, J. L., and Bloom, N. S.: Preservation and storage techniques for low-level aqueous mercury
772 speciation, *Sci. Tot. Environ.*, 337, 253-263, <https://doi.org/10.1016/j.scitotenv.2004.07.006>, 2005.

773 Patterson, B. M., Pribac, F., Barber, C., Davis, G. B., and Gibbs, R.: Biodegradation and retardation of
774 PCE and BTEX compounds in aquifer material from Western Australia using large-scale columns, *J.*
775 *Contam. Hydrol.*, 14, 261-278, [https://doi.org/10.1016/0169-7722\(93\)90028-Q](https://doi.org/10.1016/0169-7722(93)90028-Q), 1993.

776 Pirrone, N., Cinnirella, S., Feng, X., Finkelman, R.B., Friedli, H.R., Leaner, J., Mason, R., Mukherjee,
777 A.B., Stracher, G.B., Streets, D.G. and Telmer, K.: Global mercury emissions to the atmosphere from
778 anthropogenic and natural sources, *Atmos. Chem. and Phys.*, 10, 5951-5964,
779 <https://doi.org/10.5194/acp-10-5951-2010>, 2010.

780 Reis, A. T., Davidson, C. M., Vale, C., and Pereira, E.: Overview and challenges of mercury
781 fractionation and speciation in soils, *Trends Anal. Chem.*, 82, 109-117,
782 <https://doi.org/10.1016/j.trac.2016.05.008>, 2016.

783 Richard, J. H., Bischoff, C., and Biester, H.: Comparing modeled and measured mercury speciation in
784 contaminated groundwater: Importance of dissolved organic matter composition, *Environ. Sci.*
785 *Technol.*, 50, 7508-7516, <https://doi.org/10.1016/j.trac.2016.05.008>, 2016a.

786 Richard, J. H., Bischoff, C., Ahrens, C. G., and Biester, H.: Mercury (II) reduction and co-precipitation
787 of metallic mercury on hydrous ferric oxide in contaminated groundwater, *Sci. Tot. Environ.*, 539,
788 36-44, <https://doi.org/10.1016/j.scitotenv.2015.08.116>, 2016b.

789 Sentenac, P., Lynch, R. J., and Bolton, M. D.: Measurement of a side-wall boundary effect in soil
790 columns using fibre-optics sensing, *Int. J. Phys. Model. Geotech.*, 1, 35-41,
791 <https://doi.org/10.1680/ijpmg.2001.010404>, 2001.

792 Sanemasa, I.: The solubility of elemental mercury vapor in water, *Bull. Chem. Soc. Jpn.*, 48, 1795-
793 1798, <https://doi.org/10.1246/bcsj.48.1795>, 1975

794 Schroeder, W. H., and Munthe, J.: Atmospheric mercury—an overview, *Atmos. Environ.*, 32, 809-
795 822, [https://doi.org/10.1016/S1352-2310\(97\)00293-8](https://doi.org/10.1016/S1352-2310(97)00293-8), 1998.

796 Schlüter, K., Seip, H. M., and Alstad, J.: Mercury translocation in and evaporation from soil. II.
797 Evaporation of mercury from podzolized soil profiles treated with HgCl₂ and CH₃HgCl, *Soil Sediment*
798 *Contam.*, 4, 269-298, <https://doi.org/10.1080/15320389509383498>, 1995.

799 Schlüter, K.: Sorption of inorganic mercury and monomethyl mercury in an iron–humus podzol soil
800 of southern Norway studied by batch experiments, *Environ. Geol.*, 30, 266-279,
801 <https://doi.org/10.1007/s002540050156>, 1997.

802 Schnaar, G., and Brusseau, M. L.: Measuring equilibrium sorption coefficients with the miscible-
803 displacement method, *J Environ. Sci. Health A*, 48, 355-359,
804 <https://doi.org/10.1080/10934529.2013.727733>, 2013.

805 Schöndorf, T., Egli, M., Biester, H., Mailahn, W., and Rotard, W.: Distribution, Bioavailability and
806 Speciation of Mercury in Contaminated Soil and Groundwater of a Former Wood Impregnation
807 Plant, in: *Mercury Contaminated Sites*, edited by: Ebinghaus, R., Turner, R.R., de Lacerda, L.D.,
808 Vasiliev, O., Salomons, W., Springer, Berlin, Heidelberg, 181-206, https://doi.org/10.1007/978-3-662-03754-6_9, 1999.

810 Schuster, E.: The behavior of mercury in the soil with special emphasis on complexation and
811 adsorption processes-a review of the literature, *Water Air Soil Poll.*, 56, 667-680,
812 <https://doi.org/10.1007/BF00342308>, 1991.

813 Schuster, P. F., Shanley, J. B., Marvin-Dipasquale, M., Reddy, M. M., Aiken, G. R., Roth, D. A., Taylor,
814 H. E., Krabbenhoft, D. P. and DeWild, J. F.: Mercury and organic carbon dynamics during runoff
815 episodes from a northeastern USA watershed, *Water Air Soil Poll.*, 187, 89-108,
816 <https://doi.org/10.1007/s11270-007-9500-3>, 2008.

817 Schwab, L., Gallati, N., Reiter, S.M., Kimber, R.L., Kumar, N., McLagan, D.S., Biester, H., Kraemer,
818 S.M. and Wiederhold, J.G.: Mercury Isotope Fractionation during Dark Abiotic Reduction of Hg (II)
819 by Dissolved, Surface-Bound, and Structural Fe (II), *Environ. Sci. Technol.*, 57, 15243-15254,
820 <https://doi.org/10.1021/acs.est.3c03703>, 2023.

821 Skyllberg, U.: Chemical speciation of mercury in soil and sediment, in: *Environmental chemistry and*
822 *toxicology of mercury*, edited by: Liu, G., Cai, Y., Driscoll, N., Wiley & Sons Inc., Hoboken, USA, 219-
823 258, <https://doi.org/10.1002/9781118146644.ch7>, 2012.

824 Streets, D. G., Horowitz, H. M., Lu, Z., Levin, L., Thackray, C. P., and Sunderland, E. M.: Global and
825 regional trends in mercury emissions and concentrations, 2010–2015, *Atmos. Environ.*, 201, 417-
826 427, <https://doi.org/10.1016/j.atmosenv.2018.12.031>, 2019.

827 Ullrich, S. M., Tanton, T. W., and Abdrashitova, S. A.: Mercury in the aquatic environment: a review
828 of factors affecting methylation, *Crit. Rev. Environ. Sci. Technol.*, 31, 241-293,
829 <https://doi.org/10.1080/20016491089226>, 2001.

830 USEPA.: Method 1631, Revision E: Mercury in water by oxidation, purge and trap, and cold vapor
831 atomic fluorescence spectrometry, United States Environmental Protection Agency (USEPA),
832 Washington, DC, 2002.

833 USEPA.: Understanding variation in partition coefficient, K_d, values. Volume III: Review of
834 Geochemistry and Available K_d Values for Americium, Arsenic, Curium, Iodine, Neptunium, Radium,
835 and Technetium. United States Environmental Protection Agency (USEPA), Washington, DC, USA,
836 2004.

837 Van Genuchten, M. T., and Parker, J. C.: Boundary conditions for displacement experiments through
838 short laboratory soil columns, *Soil Sci. Soc. Am. J.*, 48, 703-708,
839 <https://doi.org/10.2136/sssaj1984.03615995004800040002x>, 1984.

840 Van Glubt, S., Brusseau, M. L., Yan, N., Huang, D., Khan, N., and Carroll, K. C.: Column versus batch
841 methods for measuring PFOS and PFOA sorption to geomeia. *Environ. Poll.*, 268, 115917,
842 <https://doi.org/10.1016/j.envpol.2020.115917>, 2021

843 Wiederhold, J. G., Cramer, C. J., Daniel, K., Infante, I., Bourdon, B., and Kretzschmar, R.: Equilibrium
844 mercury isotope fractionation between dissolved Hg (II) species and thiol-bound Hg, *Environ. Sci.*
845 *Technol.*, 44, 4191-4197, <https://doi.org/10.1021/es100205t>, 2010.

846 Wiederhold, J. G.: Metal stable isotope signatures as tracers in environmental geochemistry,
847 *Environ. Sci. Technol.*, 49, 2606-2624, <https://doi.org/10.1021/es504683e>, 2015.

848 Yin, Y., Allen, H. E., Li, Y., Huang, C. P., and Sanders, P. F.: Adsorption of mercury (II) by soil: effects
849 of pH, chloride, and organic matter, *J. Environ. Qual.*, 25, 837-844,
850 <https://doi.org/10.2134/jeq1996.00472425002500040027x>, 1996.

- 851 Yin, Y., Allen, H. E., Huang, C., Sparks, D. L., and Sanders, P. F.: Kinetics of mercury (II) adsorption and
852 desorption on soil, *Environ. Sci. Technol.*, 31, 496-503, <https://doi.org/10.1021/es9603214>, 1997.
- 853 Zheng, W., and Hintelmann, H.: Nuclear field shift effect in isotope fractionation of mercury during
854 abiotic reduction in the absence of light, *J. Phys. Chem. A*, 114, 4238-4245,
855 <https://doi.org/10.1021/jp910353y>, 2010.